Wafer-scale monodomain films of spontaneously-aligned single-walled carbon nanotubes

Xiaowei He[1,†], Weilu Gao[1,†], Lijuan Xie[2], Bo Li[3], Qi Zhang[1], Sidong Lei[3], John M. Robinson[1,⊥], Erik H. Hároz[4], Stephen K. Doorn[4], Weipeng Wang[3], Robert Vajtai[3], Pulickel M. Ajayan[3], W. Wade Adams[3], Robert H. Hauge[3,5] and Junichiro Kono[1,3,6,*]

[1]*Department of Electrical and Computer Engineering, Rice University, Houston, Texas 77005, USA*

[2]*College of Biosystems Engineering and Food Science, Zhejiang University, Hangzhou, Zhejiang, 310058, P. R. China.*

[3]*Department of Materials Science and NanoEngineering, Rice University, Houston, Texas 77005, USA*

[4]*Center for Integrated Nanotechnologies, Los Alamos National Laboratory, Los Alamos, New Mexico 87545, USA*

[5]*Department of Chemistry, Rice University, Houston, Texas 77005, USA*

[6]*Department of Physics and Astronomy, Rice University, Houston, Texas 77005, USA*

[†]These authors contributed equally to this work.

[⊥]Present address: Department of Physics, University of Colorado Boulder, Colorado 80302, USA.

[*]To whom correspondence should be addressed; E-mail: kono@rice.edu.

The one-dimensional character of electrons, phonons, and excitons in individual single-walled carbon nanotubes leads to extremely anisotropic electronic, thermal, and optical properties. However, despite significant efforts to develop ways to produce large-scale architectures of aligned nanotubes, macroscopic manifestations of such properties remain limited. Here, we show that large ($> \mathrm{cm}^2$) monodomain films of aligned single-walled carbon nanotubes can be prepared using slow vacuum filtration. The produced films are globally aligned within $\pm 1.5^\circ$ (a nematic order parameter of ~ 1) and are highly packed, containing 10^6 nanotubes in a cross-sectional area of $1\,\mu\mathrm{m}^2$. The method works for nanotubes synthesized by various methods, and film thickness is controllable from a few nm to ~ 100 nm. We use the approach to create ideal polarizers in the terahertz frequency range and, by combining the method with recently-developed sorting techniques, highly-aligned and chirality-enriched nanotube thin-film devices. Semiconductor-enriched devices exhibit polarized light emission, polarization-dependent photocurrent, and anisotropic conductivities and transistor action with high on/off ratios.

One of the grand challenges in nanoscience and nanotechnology is how to create macroscopic devices by assembling nano-objects while preserving their extraordinary properties. For example, individual single-walled carbon nanotubes (SWCNTs) possess unique one-dimensional properties that have stimulated much interest in diverse disciplines[1], and worldwide efforts are in progress to produce large-scale architectures of aligned SWCNTs[2,3]. Various methods have been proposed and/or demonstrated, including both postgrowth and direct-growth schemes. An early study employed a filtration method to align multiwalled CNTs, which showed strongly anisotropic properties[4]. Vertically-aligned SWCNTs can be directly grown by chemical vapor deposition (CVD)[5,6], but CNT densities in resulting films are low, making them incompatible with standard microfabrication technology; also, no type or chirality selectivity can be implemented. Some alignment has been observed by dispersing CNTs in liquid-crystal solvents that can be nematically ordered[7–9]. Stronger alignment, with a nematic order parameter, S, as high as $\sim$0.8, has been achieved by mechanically stretching a polymer film containing CNTs[10,11]; however, the existence of the matrix material as well as low CNT densities in such films severely limit the range of applications. As far as spontaneous alignment of SWCNTs is concerned, large S values have been realized only locally[12–14]; global ordering comes at the expense of S (< 0.4)[15,16]. Magnetic alignment of SWCNTs has been demonstrated[17,18], but impractically large magnetic fields are required to obtain meaningful alignment. Inkjet printing has been proven useful for creating local alignment[19], but no large-scale alignment has been reported. Recently, the Langmuir-Schaefer method was used to prepare globally-aligned, semiconductor-enriched CNTs with high surface coverage[20]; however, the degree of alignment was low, and film thickness was small and not controllable.

Hence, the current state of this field is that there is still no method available for producing large-area single-domain films of highly-aligned, densely-packed, and chirality-enriched SWCNTs, despite many years of efforts. The method we describe in the present article provides a uniform, wafer-scale ($> \text{cm}^2$) SWCNT film of an arbitrarily and precisely controllable thickness (from a few nm to $\sim$100 nm) with a high degree of alignment ($S \sim 1$) and packing ($\sim 10^6$ nanotubes in a cross-sectional area of 1 μm^2) in a well-controlled, simple, and reproducible manner, regardless of the synthesis method, metallicity, or chirality of the SWCNTs used. Furthermore, the produced films are compatible with standard microfabrication processes to fabricate various electronic and photonic devices.

Global spontaneous alignment of carbon nanotubes

The process starts with preparation of a well-dispersed CNT suspension. We disperse a CNT powder with surfactant in water to create an aqueous CNT suspension using tip sonication and ultra-centrifugation (see Methods). The second step utilizes the vacuum filtration method (Figs. 1a and 1b), which is a well-established technique for forming wafer-scale films of randomly-oriented CNTs with a controllable thickness[21]. The CNT suspension prepared in the first step is poured into the filtration funnel with a small-pore-size filter membrane, and a differential pressure across the filter membrane pushes the suspension slowly through the pores, leaving CNTs on the filter membrane. To obtain spontaneous CNT alignment, one has to satisfy three critical conditions: i) the surfactant concentration must be below the critical micelle concentration (CMC); ii) the CNT concentration must be below a threshold value, and iii) the filtration process must be well

controlled at a low speed. When these conditions are met, a wafer-scale, uniform, and aligned CNT film is formed on the filter membrane (Fig. 1b).

The film can then be transferred to any substrate in a straightforward manner after dissolving the filter membrane in a proper solvent (see Methods). The result is a large-area, semi-transparent film of aligned CNTs, as shown in the optical (Fig. 1c), scanning electron microscopy (Figs. 1d and 1e), and transmission electron microscopy (TEM) images (Figs. 1f). As the cross-sectional TEM image in Fig. 1g shows, the film is densely packed, with $\sim 10^6$ CNTs found in a cross-sectional area of 1 μm^2. Individual CNTs within the film are all aligned with each other, forming a globally ordered structure with an angle standard deviation of $\sim 1.5^\circ$ across the entire film (Fig. 1h). The film is optically polarized, i.e., linearly dichroic (Figs. 1i and 1j), being opaque to light polarized parallel to the CNT alignment direction and transparent to light polarized perpendicular to the alignment direction. Using cross-polarized microscopy, strong optical anisotropy can be demonstrated both on a macroscopic (cm) scale (Fig. 1i) and a microscopic (μm) scale (Fig. 1j), reflecting the global and local CNT alignment, respectively. Finally, the film can be easily patterned using conventional photolithography techniques (Fig. 1j).

Spectroscopy of spontaneously aligned carbon nanotubes

Figure 2 summarizes results of spectroscopic characterization measurements of aligned CNT films. Figure 2a shows polarized Raman spectra for a 15-nm-thick aligned film of arc-discharge SWCNTs with an average tube diameter of 1.4 nm, taken with an excitation wavelength of 514 nm in

two polarization configurations. The data was analyzed using standard equations for the angular dependence of SWCNT Raman spectra[9] to deduce the value of S, which was 0.96 for this particular film (see also Supplementary Information Section 3). Electromagnetic response of this film was strongly polarization dependent in the whole spectral range, from the terahertz (THz) to the visible, as shown in Fig. 2b with the energy axis on a logarithmic scale. In particular, there is no detectable attenuation within experimental errors for the perpendicular polarization in the entire THz/infrared range (< 1 eV) whereas there is a prominent, broad peak at $\sim$0.02 eV in the parallel case due to the plasmon resonance[22]. Figure 2c plots the same spectra with the energy axis on a linear scale, to more clearly show interband absorption — i.e., the first two interband transitions for semiconducting nanotubes (E_{11}^S and E_{22}^S) and the first interband transition in metallic nanotubes (E_{11}^M). Due to the exceptionally high degree of CNT alignment, these peaks are completely absent for the perpendicular polarization, and instead, a broad absorption feature is observed in an intermediate energy region between the E_{11}^S and E_{22}^S peaks. We attribute this feature to the cross-polarized and depolarization-suppressed E_{12}^S/E_{21}^S absorption peak[23], previously detected in polarized photoluminescence excitation spectroscopy experiments in individualized CNTs[24,25].

As noted previously[26], the exceptionally strong polarization-dependence of THz transmission through aligned CNT films can be utilized to form an ideal THz polarizer with extremely large extinction ratios (ER); ER = $T_\parallel/T_\perp$, where $T_\parallel$ ($T_\perp$) is the transmittance for the parallel (perpendicular) polarization. Figure 2d shows time-domain waveforms of THz radiation transmitted through an aligned arc-discharge SWCNT film on an intrinsic silicon substrate for polarizations parallel and perpendicular to the alignment direction, together with a reference waveform obtained

for the substrate alone. The data for the perpendicular case completely coincides with the reference trace, i.e., no attenuation occurs within the SWCNT film. On the other hand, there is significant attenuation for the parallel case. Note that the THz beam had a mm^2 size, thus probing a macroscopic area. Figure 2e shows a more detailed polarization-angle dependence of THz attenuation, plotted as a function of the angle between the THz polarization and the nanotube alignment direction. The attenuation anisotropy allows us to calculate the value of S in a straightforward manner[26], which also agrees with the value obtained by Raman spectroscopy. The value of ER monotonically increases with the film thickness at $\sim$12 dB/100 nm, while high values of S are maintained even for relatively thick films (Fig. 2f).

Universal applicability of vacuum filtration

Our method of making aligned films is universally applicable to different types of SWCNTs. Table 1 lists seven representative suspensions used, which contained SWCNTs synthesized by the arc-discharge, CVD, CoMoCAT, and HiPco methods. Here, d_t is the average nanotube diameter, and l_t is the average nanotube length measured by atomic force microscopy (see Supplementary Fig. 8). For dispersing CNTs, we used sodium deoxycholate (DOC) for Suspensions #1 and #4$-$#7 and sodium dodecylbenzenesulfonate (SDBS) for #2, as surfactant. Pre-functionalized, water-soluble SWCNTs were used in Suspension #3 (see Supplementary Information Section 1); successful formation of aligned films made from this suspension indicates that surfactant is not a crucial element for spontaneous CNT alignment, as long as the CNTs are well dispersed in the suspension. Note, however, that CNTs in all these suspensions were negatively charged, and thus,

Table 1: Different types of CNT suspensions used for making aligned films. d_t: average tube diameter, l_t: average tube length, S_{THz} (S_{Raman}): nematic order parameter obtained from THz (Raman) measurements, DOC: sodium deoxycholate, and SDBS: sodium dodecylbenzenesulfonate. †Suspension #3 contained arc-discharge-synthesized CNTs that were functionalized by polyaminobenzene sulfonic (PABS) acid. ‡Suspension #4 contained TUBALL$^{\mathrm{TM}}$ nanotubes from OCSiAl (http://ocsial.com/en/product/tuball/). *Suspension #6 was enriched in (6,5) SWCNTs. $^{\top}$Suspension #7 was enriched in (7,6), (8,6), and (10,5) SWCNTs. $^{\perp}$Suspension #5, #6, and #7 did not have high enough carrier densities to show strong enough THz attenuation to determine S_{THz}.

Suspension	Synthesis	Surfactant	d_t (nm)	l_t (nm)	S_{THz}	S_{Raman}
#1	Arc-Discharge	DOC	1.4	227	$\sim$1	0.96
#2	Arc-Discharge	SDBS	1.4	246	$\sim$1	0.94
#3	Arc-Discharge	N/A†	1.4	295	0.77	0.72
#4	CVD‡	DOC	1.8	307	0.9	0.85
#5	CoMoCAT	DOC	$\sim$1	166	N/A$^{\perp}$	0.73
#6	CoMoCAT*	DOC	0.73	420	N/A$^{\perp}$	0.75
#7	HiPco$^{\top}$	DOC	$\sim$0.9	298	N/A$^{\perp}$	0.72

it is currently not clear whether CNT alignment can be achieved with positively charged or neutral surfactants. Also listed in Table 1 are nematic order parameters, S_{THz} and S_{Raman}, determined through THz and Raman measurements, respectively; only S_{Raman} is shown for Suspensions #5, #6, and #7 because the films from these suspensions did not have sufficiently high carrier densities to show strong enough THz attenuation for determining S_{THz}. There is no obvious relationship observed between the structure parameters of SWCNTs and the achieved values of S_{THz} and S_{Raman}. Arc-discharge SWCNTs tend to align more strongly than other types of nanotubes, but further systematic studies using diameter- and length-sorted samples are needed to clarify whether this difference comes from their differences in d_t, l_t, or d_t/l_t.

Alignment mechanism

The strikingly high values of S achieved precludes the possibility that the alignment mechanism is based on three-dimensional (3D) nematic ordering of rigid rods, for which Onsager's theory predicts an upper limit of S = 0.79[15,27]. Formation of a 3D nematic liquid-crystal phase of CNTs would require a high CNT concentration[8], with a threshold value ~5 mg/mL for CNTs with l_t/d_t $\sim 10^3$. This condition was not met in our case (typical CNT concentration $\sim$ 15 μg/mL, and l_t/d_t = 150-550), suggesting that a different alignment mechanism is at work. A clue for the mechanism comes from our observation that the degree of alignment was sensitive to the hydrophobicity of the filter membrane surface, similar to a prior report on 2D nematic ordering of DNA-wrapped CNTs[12]. Alignment was achieved only when the filter membrane had a hydrophilic coating layer (PVP). Additionally, control of the flow rate, CNT concentration, and surfactant concentration was

crucial. Based on these observations, we propose that CNT alignment occurs in a 2D manner. Hydrophilic PVP coating makes the filter paper surface negatively charged during filtration, and as a result, negatively charged CNTs in the suspension are repelled from the surface. At the same time, CNTs feel van der Waals attraction from uncoated regions of the membrane surface. The competition of these two forces creates a potential minimum near the surface, where CNTs accumulate, interact with each other, and form an ordered 2D phase[12]. Because the formation of ordered structure requires horizontal (i.e., in-plane) rotation of CNTs in a finite time period to arrange themselves within the 2D layer, an appropriate filtration speed and CNT concentration are important. Furthermore, the surfactant concentration affects the charge density on the PVP layer, which in turn influences the electrostatic repulsion potential, while at the same time the suspension viscosity depends on the surfactant concentration, which influences the rotational motion of CNTs in the 2D layer. A more detailed discussion on the influences of all critical factors on CNT alignment is provided in Supplementary Information Section 4.

2D surface confinement is a novel route towards fabricating ordered nanostructures[12,20,28,29]. In the Langmuir-Schaefer method[20], for example, nano-objects initially float on the surface of water, i.e., confined at the interface between air and water, and eventually form an ordered phase. However, CNT concentrations used in previous studies were extremely low (e.g., 0.1-1 μg/mL[12]). The obtained films of aligned CNTs remained small[12] and thin (limited to a monolayer[12] or several layers[20]), and the degree of alignment was low[20] (e.g., the Raman G-peak intensity anisotropy $\approx$ 10, compared to $\sim$160 in our case). In addition to stronger alignment, our films have other distinct advantages. First, unlike the previous 2D ordering studies, we can continue accumulating aligned

CNTs to achieve optically think films ($\sim$100 nm); the fact that we get S values higher than the rigid-rod limit to such thicknesses suggests that some attractive interaction is present between the tubes when the surfactant concentration is low. Second, the cross-sectional areal density is as high as 10^6 nanotubes/μm^2, orders of magnitude larger than any previous reports[12,20,28,29]. These two advantages indicate that a transition from 2D-like to 3D-like ordering occurs as CNTs gradually accumulate on the surface; once there is an aligned layer, the CNTs that follow tend to align with the already-existing alignment direction. Finally, there is in principle no limitation on the achievable area of aligned films; practically, it is only limited by the size of the filter membrane.

Devices based on aligned carbon nanotube films

With the ultimate aim of developing optoelectronic technologies based on aligned single-chirality SWCNTs, we used CNT suspensions enriched in specific types and chiralities in making aligned CNT films (e.g., Suspension #6 in Table 1) and fabricated light emission and detection devices (Fig. 3). Recent advances in postgrowth separation and sorting techniques allow us to prepare suspensions of specific chirality, (n,m), SWCNTs at large enough quantities for making macroscopic films. Here, we used the aqueous two-phase extraction method[30–32] to enrich (6,5) SWCNTs. Figure 3a shows photographs of the prepared suspension and film, while Figs. 3b and 3c show the optical absorption and photoluminescence excitation spectra of the enriched suspension. There are trace amounts of (8,4) and (9,1) SWCNTs in the suspension, but it is clear that the majority of the nanotubes are (6,5) species. The fabricated (6,5) film showed strongly polarized photoluminescence (Figs. 3d and 3e). This macroscopic manifestation of light emission anisotropy not only

provides evidence that the CNTs in the film are highly aligned but also proves that there are very few residual metallic tubes, which are known to be efficient photoluminescence quenchers when in contact with semiconducting nanotubes. This result opens up new possibilities of developing CNT-based light sources for producing polarized monochromatic radiation.

Our photodetector was a two-terminal device (see Methods and Fig. 3f), which exhibited strongly polarization-sensitive photosignal (Fig. 3g). The polarization ratio of photosignal magnitude was $\sim$2:1. The responsivity of the photodetector was estimated to be $\sim$0.1 V/W, after taking into account the actual power absorption of $\sim$3.1 mW when the light polarization is parallel to the CNT alignment direction. Compared to previous photodetectors with the same device architecture but consisting of a mixture of metallic and semiconducting SWCNTs[33], the responsivity of the current photodectector has been enhanced by at least three times, most likely due to the removal of metallic tubes. It should be noted, however, that the current device design has not been fully optimized. With proper thermal management through selection and adjustment of substrates and other critical elements, the detector performance can be further improved[34].

Finally, we fabricated electronic devices out of aligned CNT films using standard microfabrication techniques and tested their conductivities and transistor performance (Fig. 4). First, we observed strong conductivity anisotropy in Hall-bar devices made of aligned unsorted arc-discharge CNTs at room temperature (Figs. 4a to 4b). The ratio of conductivity between the parallel and perpendicular directions is as high as 60 (Fig. 4b). The conductivity along the alignment direction was 2500 S/cm; this value is much higher than the typical conductivities reported for aligned films

made from chemical vapor deposition grown CNTs, which are only $\sim$10 S/cm along the alignment direction[35] because of their low densities. Furthermore, our films are more conducting than previously reported dense random-network films, whose conductivities are typically on the order of hundreds of S/cm without intentional doping[36,37], while our films are not intentionally doped.

In addition, we investigated transistor behaviors of a (6,5)-enriched aligned film (Fig. 4c). As shown in Figs. 4d and 4e, the on-current density of the transistor in the parallel (perpendicular) direction is $\sim$2 nA/μm ($\sim$80 pA/μm), indicating that the on-current density can be improved through aligning CNTs in one direction. Note that these nearly intrinsic semiconducting films are naturally much less conducting than purely metallic films or films with mixed electronic types. As shown previously[38], the on-current density can also be enhanced by using larger-diameter nanotubes, which is also demonstrated by our transistor based on semiconductor-enriched arc-discharge CNTs with an average diameter of 1.4 nm (Fig. 4e). The device shows an enhancement of on-current density by $\sim$50 times compared to the (6,5) CNT transistor at the same drain-source voltage. The on-off ratios of our transistors are around 10^3, which is comparable to previous results for transistors made of aligned CNT films. The relatively low on-off ratio is ascribed to the charge screening effect caused by the high packing of CNTs in one direction[20]. It can be potentially overcome by using a high-κ dielectric material or using a top-gate architecture.

Conclusions

We have developed a new process to produce a wafer-scale (i.e., inch-size) film of aligned CNTs of an adjustable thickness. This method works for CNTs synthesized by various methods. The produced large-area films will produce a range of new opportunities not only in fundamental research of physics, chemistry, and materials science but also applications in electronics, optoelectronics, sensing, imaging, and medicine. We already demonstrated terahertz/infrared polarizers using metal-semiconductor mixed CNTs, thin-film transistors using semiconducting CNTs, polarized light emission devices using semiconducting CNTs, and polarization-sensitive photodetectors.

Methods

CNT suspension preparation. Two batches of arc-discharge SWCNTs (P2-SWNT and P8-SWNT) with an average diameter of 1.4 nm were purchased from Carbon Solutions, Inc. Two types of CoMoCAT SWCNTs (CG 200 and SG 65i) were purchased from Sigma-Aldrich; the former had a wide diameter distribution (0.7-1.4 nm) whereas the latter was enriched in (6,5) SWCNTs with $\sim$90% purity. CVD-grown TUBALL$^{\text{TM}}$ CNTs, which were 75% SWCNTs, were obtained from OCSiAl and had an average diameter of $\sim$1.8 nm. HiPco SWCNTs (batch # 195.5), with a diameter range of 0.9-1 nm, were used after purification and diameter sorting. As surfactants for CNT dispersion, we used sodium deoxycholate (DOC, Sigma-Aldrich) and sodium dodecylbenzenesulfonate (SDBS, Sigma-Aldrich). All CNTs (except for P8-SWNT) were initially dispersed in either 1% (wt./vol.) DOC or 0.4% (wt./vol) SDBS by bath sonication (Cole-Parmer 60-W ultrasonic cleaner, model #08849-00) for 5-10 minutes at a starting concentration of 0.2-0.8 mg/mL. The

obtained suspension was then further sonicated with a tip sonicator (XL-2000 Sonicator, Qsonica, LLC., 1/4" probe, $\sim$30 watts) for 45-60 minutes. The suspension was cooled in an ice water bath during the sonication. Next, the suspension was centrifuged for 1 hour at 38000 rpm (Sorvall Discovery 100SE Ultracentrifuge using a Beckman SW-41 Ti swing bucket rotor) to remove large bundles of CNTs. After centrifugation, the upper 60% of the supernatant was collected and then diluted with Nanopure water. The concentration of surfactant was diluted below its critical micelle concentration (CMC). Depending on the type of CNTs used, the final concentration of DOC before film making varied from 0.02% to 0.1%, and the final concentration of SDBS was $\sim$0.02%.

Vacuum filtration. Well-dispersed CNT suspension with dilute CNTs ($\sim$1-15 μg/mL) and dilute surfactant (below CMC) was filtered though a vacuum filtration system in a well-controlled manner. Polycarbonate filter membranes (Nuclepore Track-Etched Polycarbonate Hydrophilic Membranes) with different pore sizes from 50 to 200 nm were used. The filtration speed was kept low and controlled in a range of 1-2 mL/hour. The pressure applied to the system by vacuum pumping was monitored through sensitive pressure gauges. A speeding-up procedure was performed at the end of the filtration process to dry the film quickly. Before transferring the film onto another substrate, the film was pumped on for an additional 15-30 minutes.

Transfer and characterization. For characterization and device fabrication, films were transferred onto solid substrates (e.g., SiO_2/Si and quartz) using a wet transfer process[13], in which the polycarbonate filter membrane was dissolved away with organic solvent (*N*-methyl-2-pyrrolidone or chloroform). The films were then thoroughly washed by acetone and nanopure water; subsequent X-ray photoelectron spectroscopy experiments did not detect any residual surfactants

(see Supplementary Fig. 10). Properties of fabricated CNT films were characterized by various methods. Anisotropic optical transmission on a large scale was characterized by polarized optical microscopy in both co-polarized and cross-polarized configurations. Alignment structure on micro- and nano-meter scales was examined by scanning electron microscopy (JEOL 6500F Scanning Electron Microscope) and transmission electron microscopy (JEOL 2100 Field Emission Gun Transmission Electron Microscope). The quality of CNT alignment was characterized in terms of local and global nematic order parameters based on polarized Raman spectroscopy (RENISHAW inVia Raman Microscope) and terahertz transmission spectroscopy (a home-made time-domain THz spectroscopy system). Film thicknesses were measured by atomic force microscopy (Bruker Multimode 8). The average lengths of CNTs in suspensions were measured by atomic force microscopy (see Supplementary Fig. 8). Photoluminescence excitation spectra of the single-chirality (6,5) CNT suspension and polarized photoluminescence of the single-chirality (6,5) films were measured with a home-made photoluminescence excitation spectroscopy setup.

Device fabrication. i) Photodetector: Aligned (6,5) nanotube films were cut into ribbons and then transferred to glass substrates. Two electrodes were formed by sputtering 50-nm gold with a shadow mask at the two ends of a ribbon. A 660-nm laser beam with a maximum power of $\sim$50 mW was incident on and near a gold-CNT junction. A half-wave plate was used to rotate the polarization of the incident light beam without changing the incident power. The generated photo-voltage was amplified by a Stanford Research SR560 voltage preamplifier and then fed into a Stanford Research SR830 lock-in amplifier. ii) Hall-bar device and field effect transistor: An aligned nanotube film was transferred onto a substrate comprised of heavily doped silicon (acting

as a global back gate for the field effect transistors) and 285-nm thick layer of thermal silicon oxide (acting as the insulating layer). The first photolithography step was to define the electrode area with Shipley Microposit S1813 photoresist. The electrodes were defined and fabricated by lifting off electron-beam-evaporated titanium (1 nm) / palladium (10 nm) / gold (20 nm). The next step was to define a Hall bar structure with one channel parallel and the others perpendicular to the CNT alignment direction, as shown in Figs. 4a and 4c. Anisotropic transport measurements of the aligned film consisting of unsorted arc-discharge CNTs were performed under ambient conditions via four-terminal sensing using a Keithley 2400 source meter. Field effect transistor measurements were performed under vacuum ($\sim 1 \times 10^{-5}$ torr), using a Keithley 2634B source meter (for the source-drain voltage) and a Keithley 2400 source meter (for the gate voltage).

1. Jorio, A., Dresselhaus, G. & Dresselhaus, M. S. (eds.) *Carbon Nanotubes: Advanced Topics in the Synthesis, Structure, Properties and Applications* (Springer, Berlin, 2008).

2. Ma, Y., Wang, B., Wu, Y., Huang, Y. & Chen, Y. The production of horizontally aligned single-walled carbon nanotubes. *Carbon* **49**, 4098–4110 (2011).

3. Liu, B., Wang, C., Liu, J., Che, Y. & Zhou, C. Aligned carbon nanotubes: From controlled synthesis to electronic applications. *Nanoscale* **5**, 9483–9502 (2013).

4. de Heer, W. A. *et al.* Aligned carbon nanotube films: Production and optical and electronic properties. *Science* **268**, 845–847 (1995).

5. Murakami, Y. *et al.* Growth of vertically aligned single-walled carbon nanotube films on quartz substrates and their optical anisotropy. *Chem. Phys. Lett.* **385**, 298–303 (2004).

6. Pint, C. L., Xu, Y., Pasquali, M. & Hauge, R. H. Formation of highly dense, aligned ribbons and ultra-thin films of single-walled carbon nanotubes from carpets. *ACS Nano* **2**, 1871–1878 (2008).

7. Lynch, M. D. & Patrick, D. L. Organizing carbon nanotubes with liquid crystals. *Nano Lett.* **2**, 1197–1201 (2002).

8. Lagerwall, J. P. F. & Scalia, G. Carbon nanotubes in liquid crystals. *J. Mater. Chem.* **18**, 2890–2898 (2008).

9. Zamora-Ledezma, C. *et al.* Anisotropic thin films of single-wall carbon nanotubes from aligned lyotropic nematic suspensions. *Nano Lett.* **8**, 4103–4107 (2008).

10. Kim, Y., Minami, N. & Kazaoui, S. Highly polarized absorption and photoluminescence of stretch-aligned single-wall carbon nanotubes dispersed in gelatin films. *Appl. Phys. Lett.* **86**, 073103 (2005).

11. Shaver, J. *et al.* Magnetic brightening of carbon nanotube photoluminescence through symmetry breaking. *Nano Lett.* **7**, 1851–1855 (2007).

12. Mclean, R. S., Huang, X., Khripin, C., Jagota, A. & Zheng, M. Controlled two-dimensional pattern of spontaneously aligned carbon nanotubes. *Nano Lett.* **6**, 55–60 (2006).

13. Dan, B., Ma, A. W. K., Hároz, E. H., Kono, J. & Pasquali, M. Nematic-like alignment in SWNT thin films from aqueous colloidal suspensions. *Industr. Eng. Chem. Res.* **51**, 10232–10237 (2012).

14. Oh, J. Y. *et al.* Easy preparation of self-assembled high-density buckypaper with enhanced mechanical properties. *Nano Lett.* **15**, 190–197 (2015).

15. Puech, N. *et al.* Highly ordered carbon nanotube nematic liquid crystals. *J. Phys. Chem. C* **115**, 3272–3278 (2011).

16. Zakri, C. *et al.* Liquid crystals of carbon nanotubes and graphene. *Phil. Trans. R. Soc. Lond. A* **371**, 1988 (2013).

17. Walters, D. A. *et al.* In-plane-aligned membranes of carbon nanotubes. *Chem. Phys. Lett.* **338**, 14–20 (2001).

18. Zaric, S. *et al.* Estimation of magnetic susceptibility anisotropy of carbon nanotubes using magneto-photoluminescence. *Nano Lett.* **4**, 2219–2221 (2004).

19. Beyer, S. T. & Walus, K. Controlled orientation and alignment in films of single-walled carbon nanotubes using inkjet printing. *Langmuir* **28**, 8753–8759 (2012).

20. Cao, Q. *et al.* Arrays of single-walled carbon nanotubes with full surface coverage for high-performance electronics. *Nat. Nanotech.* **8**, 180–186 (2013).

21. Wu, Z. *et al.* Transparent, conductive nanotube films. *Science* **305**, 1273–1276 (2004).

22. Zhang, Q. *et al.* Plasmonic nature of the terahertz conductivity peak in single-wall carbon nanotubes. *Nano Lett.* **13**, 5991–5996 (2013).

23. Ajiki, H. & Ando, T. Aharonov-bohm effect in carbon nanotubes. *Physica B* **201**, 349–352 (1994).

24. Miyauchi, Y., Oba, M. & Maruyama, S. Cross-polarized optical absorption of single-walled nanotubes by polarized photoluminescence excitation spectroscopy. *Phys. Rev. B* **74**, 205440 (2006).

25. Lefebvre, J. & Finnie, P. Polarized photoluminescence excitation spectroscopy of single-walled carbon nanotubes. *Phys. Rev. Lett.* **98**, 167406 (2007).

26. Ren, L. *et al.* Carbon nanotube terahertz polarizer. *Nano Lett.* **9**, 2610–2613 (2009).

27. Onsager, L. The effects of shape on the interaction of colloidal particles. *Ann. N.Y. Acad. Sci.* **51**, 627–659 (1949).

28. Yang, P. Nanotechnology: Wires on water. *Nature* **425**, 243–244 (2003).

29. Sharma, R., Lee, C. Y., Choi, J. H., Chen, K. & Strano, M. S. Nanometer positioning, parallel alignment, and placement of single anisotropic nanoparticles using hydrodynamic forces in cylindrical droplets. *Nano Lett.* **7**, 2693–2700 (2007).

30. Khripin, C. Y., Fagan, J. A. & Zheng, M. Spontaneous partition of carbon nanotubes in polymer-modified aqueous phases. *J. Am. Chem. Soc.* **135**, 6822–6825 (2013).

31. Subbaiyan, N. K. *et al.* Role of surfactants and salt in aqueous two-phase separation of carbon nanotubes toward simple chirality isolation. *ACS Nano* **8**, 1619–1628 (2014).

32. Fagan, J. A. *et al.* Isolation of specific small-diameter single-wall carbon nanotube species via aqueous two-phase extraction. *Adv. Mat.* **26**, 2800–2804 (2014).

33. Nanot, S. *et al.* Broadband, polarization-sensitive photodetector based on optically-thick films of macroscopically long, dense, and aligned carbon nanotubes. *Sci. Rep.* **3**, 1335 (2013).

34. He, X. *et al.* Photothermoelectric p-n junction photodetectors with intrinsic polarimetry based on macroscopic carbon nanotube films. *ACS Nano* **7**, 7271–7277 (2013).

35. Jakubinek, M. B. *et al.* Thermal and electrical conductivity of tall, vertically aligned carbon nanotube arrays. *Carbon* **48**, 3947–3952 (2010).

36. Bekyarova, E. *et al.* Electronic properties of single-walled carbon nanotube networks. *J. Am. Chem. Soc.* **127**, 5990–5995 (2005).

37. Zhang, D. *et al.* Transparent, conductive, and flexible carbon nanotube films and their application in organic light-emitting diodes. *Nano Lett.* **6**, 1880–1886 (2006).

38. Chen, Z., Appenzeller, J., Knoch, J., Lin, Y. & Avouris, P. The role of metal-nanotube contact in the performance of carbon nanotube field-effect transistors. *Nano Lett.* **5**, 1497–1502 (2005).

Acknowledgements This work was supported by the Basic Energy Sciences (BES) program of the US Department of Energy through Grant No. DE-FG02-06ER46308 (for the preparation and characterization of aligned carbon nanotube films) and the Robert A. Welch Foundation through Grant No. C-1509 (for terahertz and infrared characterization). S.K.D. and E.H.H. acknowledge support from the LANL LDRD program. Portions of this work were performed at the Center for Integrated Nanotechnologies, a U.S. Department of Energy, Office of Science user facility. We thank Hirotaka Kasai, Ahmed Zubair, Cody Sewell, Sean Peters, and Takaya Higashira for their assistance with THz characterization measurements and Inna Kurganskaya, Andreas Lüttge, Robert Headrick, and Matteo Pasquali for helpful discussions.

Competing interests The authors declare no competing financial interests.

Author contributions X.H. and W.G. developed the process of making aligned CNT films, performed most of the characterization experiments, and analyzed the data obtained, under the supervision and guidance of W.W.A., R.H.H., and J.K. L.X. prepared chirality-enriched SWCNT suspensions, in collaboration with E.H.H. and S.K.D. B.L. made the AFM measurements and B.L. and W.W. performed TEM imaging, under the advisement of R.V. and P.M.A. Q.Z. and J.M.R. participated in the THz and infrared spectroscopy measurements. S.L. helped characterize the FET devices. X.H., W.G., and J.K. wrote the manuscript. All authors discussed the results and commented on the manuscript.

Correspondence Correspondence and requests for materials should be addressed to Junichiro Kono (email: kono@rice.edu).

Figure 1 Fabrication and characterization of wafer-scale monodomain films of aligned carbon nanotubes. **a**, A CNT suspension goes through a standard vacuum filtration system. For spontaneous CNT alignment to occur, the filtration speed must be kept low, and the CNTs must be well dispersed in the suspension. **b**, A wafer-scale, uniform CNT film is formed on the filter membrane. **c**, An optical image of the produced film after being transferred to a transparent substrate by dissolving the filter membrane. **d**, A scanning electron microscopy image, **e**, a high-resolution scanning electron microscopy image, and **f**, a top-view transmission electron microscopy image of the film, showing strong alignment and high density. **g**, A high-resolution cross-sectional transmission electron microscopy image, further showing a high cross-sectional areal density $\sim 10^6/\mu\text{m}^2$. **h**, Angular distribution of CNTs within a 1-cm^2 area of the film, with a standard deviation of 1.5°, determined by SEM image analysis. The film is opaque to light polarized parallel to the CNT alignment direction and transparent to light polarized perpendicular to the alignment direction on a macroscopic scale (**i**) and a microscopic scale (**j**). Note also that the film can be easily patterned using conventional photolithography techniques, as shown in **j**.

Figure 2 Characterization of aligned carbon nanotube films through polarization-dependent optical spectroscopy. **a**, Raman spectra for an aligned arc-discharge carbon nanotube film for two configurations. In the VV (HH) configuration, both the incident and scattered beams are polarized parallel (perpendicular) to the nanotube alignment direction. **b**, Polarization-dependent attenuation spectra in a wide spectral range, from

the THz/far-infrared to the visible. **c**, Expanded view of **b**, showing interband transitions. **d**, Time-domain THz waveforms of transmitted THz radiation for parallel and perpendicular polarizations. The data for the perpendicular case completely overlaps with the reference trace, i.e., no attenuation is detectable. The THz beam had a beam size of mm^2 size, thus probing a macroscopic area. **e**, Attenuation as a function of the angle between the THz polarization and the nanotube alignment direction. **f**, The nematic order parameter (S), left axis, deduced from the THz attenuation data, and the extinction ratio (ER), right axis, as a function of film thickness.

Figure 3 Optoelectronic devices made from aligned and (6,5)-enriched carbon nanotube films. **a**, Photographs of a (6,5)-enriched suspension (left) and a fabricated large-area aligned film (right). **b,c**, Photoluminescence excitation (**b**) and optical absorption (**c**) spectra of the (6,5)-enriched suspension. **d**, Strongly-polarized photoluminescence spectra for an aligned and (6,5)-enriched CNT film, showing stronger emission polarized parallel to the CNT alignment direction. **e**, Polar plot of the intensity of the emitted photoluminescence from the aligned and (6,5)-enriched CNT film. **f**, Schematic diagram showing the photodetector device fabricated from an aligned and (6,5)-enriched CNT film. **g**, Polarization-dependent photovoltage observed for the device shown in **f**, with an improved responsivity $\sim$0.1 V/W compared with a structurally similar device made of unsorted SWCNTs[33].

Figure 4 Electronic devices made from aligned carbon nanotube films. **a**, Photograph and schematic diagrams of Hall-bar devices with channel length $\sim$ 5 mm and channel width $\sim$ 0.5 mm used to characterize the macroscopic anisotropic transport of charge carriers in an aligned film consisting of unsorted arc-discharge CNTs via four-terminal measurements. **b**, Voltage-current relationship of the Hall-bar devices when the current flow is parallel and perpendicular to the CNT alignment direction, showing extremely anisotropic conductivities. **c**, False-color scanning electron microscopy images of a thin-film transistor with channel width $\sim$5 μm and channel length $\sim$30 μm made from an aligned and (6,5)-enriched CNT film. **d**, The source-drain current versus source-drain voltage at zero gate voltage of the transistor showing anisotropic conductivities of the aligned (6,5)-enriched thin-film transistor. **e**, The source-drain current at a source-drain voltage of 1 V versus gate voltage of the (6,5)-enriched transistor showing large and anisotropic transistor action. The on-current density is enhanced by 50 times in a transistor made from larger-diameter semiconductor-enriched arc-discharge SWCNTs.

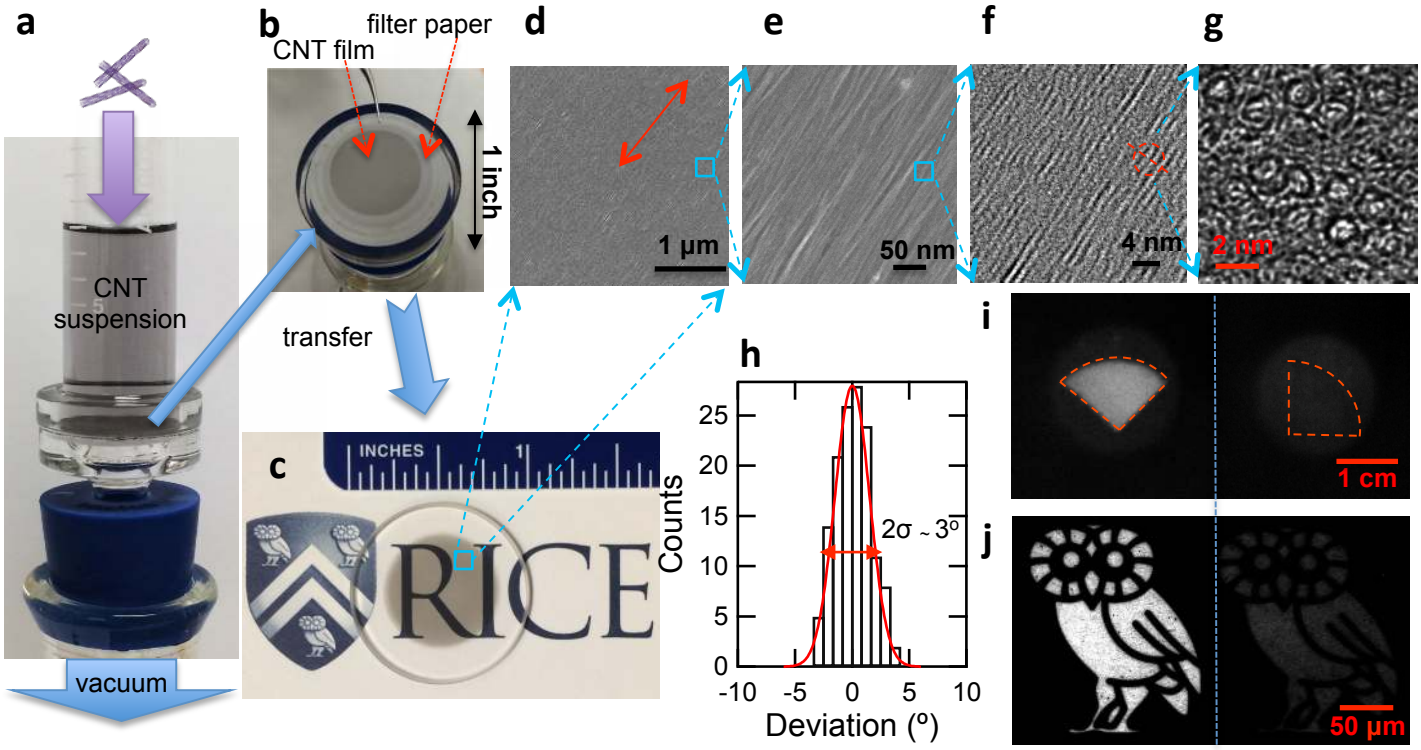
a
b
filter paper
CNT film
1 inch
CNT
suspension
transfer
vacuum
c
INCHES
RICE
d
1 μm
e
50 nm
f
4 nm
g
2 nm
h
Counts
25
20
15
10
5
0
-10
-5
0
5
10
Deviation (°)
2σ ~ 3°
i
1 cm
j
50 μm

Figure 1

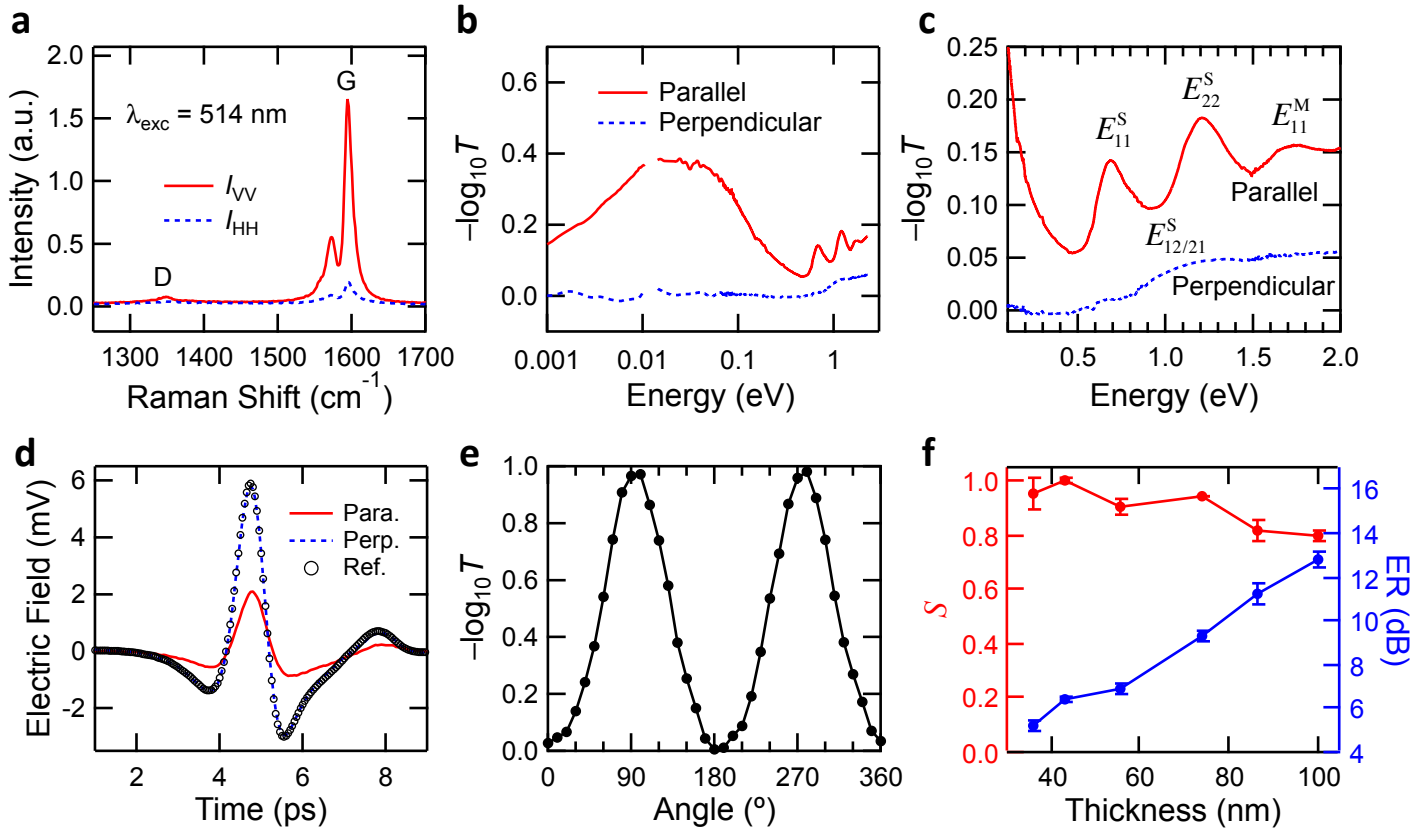
a
Intensity (a.u.)
λexc = 514 nm
IVV
IHH
G
D
Raman Shift (cm-1)
b
−log10T
Parallel
Perpendicular
Energy (eV)
c
−log10T
E11S
E22S
E11M
E12/21S
Parallel
Perpendicular
Energy (eV)
d
Electric Field (mV)
Para.
Perp.
Ref.
Time (ps)
e
−log10T
Angle (°)
f
S
ER (dB)
Thickness (nm)

Figure 2

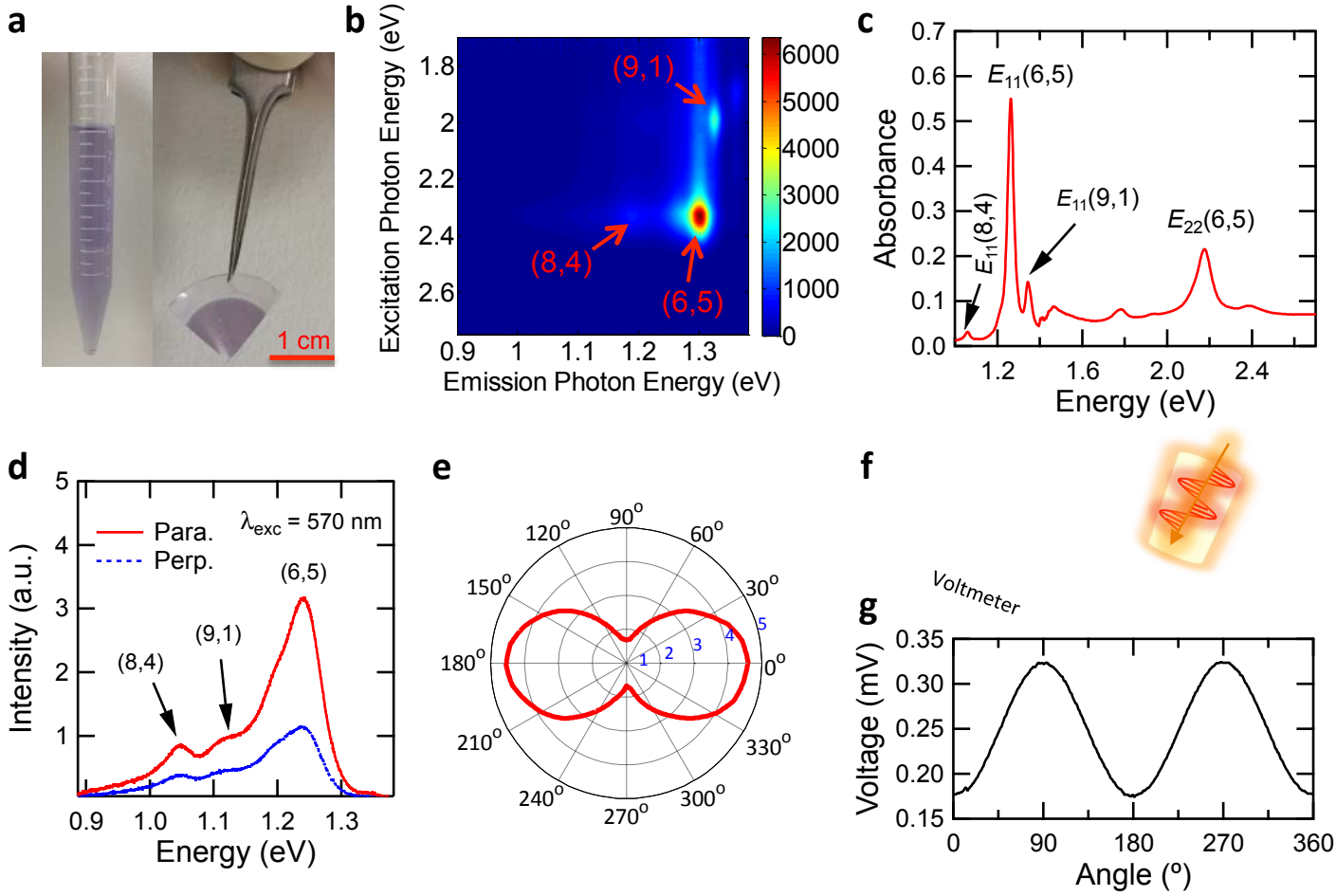
a
1 cm
b
Excitation Photon Energy (eV)
Emission Photon Energy (eV)
(9,1)
(8,4)
(6,5)
c
Absorbance
Energy (eV)
E_{11}(6,5)
E_{11}(9,1)
E_{22}(6,5)
E_{11}(8,4)
d
Intensity (a.u.)
Energy (eV)
Para.
Perp.
λ_{exc} = 570 nm
(6,5)
(9,1)
(8,4)
e
f
Voltmeter
g
Voltage (mV)
Angle (°)

Figure 3

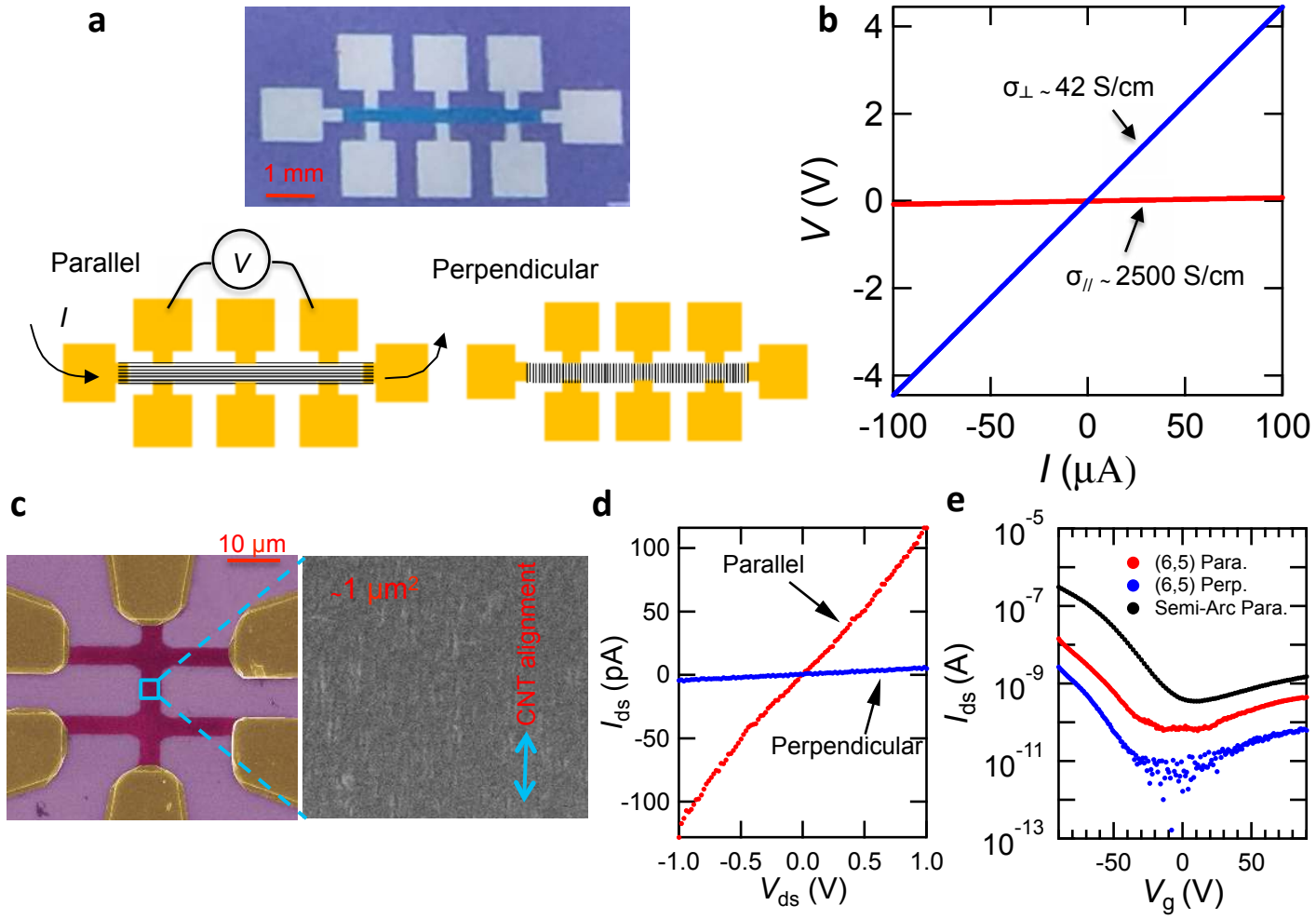
a
1 mm
Parallel
V
I
Perpendicular
b
σ⊥ ~ 42 S/cm
σ// ~ 2500 S/cm
V (V)
I (μA)
c
10 μm
~1 μm²
CNT alignment
d
Parallel
Perpendicular
I_ds (pA)
V_ds (V)
e
(6,5) Para.
(6,5) Perp.
Semi-Arc Para.
I_ds (A)
V_g (V)

Figure 4